

Fluorescence-Enabled Colored Bilayer Subambient Radiative Cooling Coatings

Xue Ma, Yang Fu, Danjun Liu, Ning Yang, Jian-Guo Dai, and Dangyuan Lei*

Passive daytime radiative cooling has emerged as a promising green technology for the thermal management of buildings, vehicles, textiles, and electronics. Typically, both high solar reflectance and high thermal emissivity are prerequisites to achieve sufficient daytime cooling. However, colored radiative cooling materials are facing the dilemma of introducing visible light absorption, leading to challenges in balancing cooling and aesthetic demands. Here, three colored bilayer radiative cooling coatings, each comprised of a white base layer and a colored top layer with fluorescence enhancement are fabricated. Three phosphors (Sr₂Si₅N₈:Eu²⁺, Y₃Al₅O₁₂:Ce³⁺, and (Ba,Sr)SiO₄:Eu²⁺) are employed with respective photoluminescence quantum yields (PLQYs) of 81%, 95.8%, and 91.0% as the colored pigment in the top layer. To mitigate the contradiction between coloration and solar reflectance, SiO₂ microspheres are introduced into the top layer and utilize their Mie-resonance-based multiple scattering to increase the photoluminescent (PL) properties of the phosphors, which jointly boosts the effective solar reflectance (ESR) of the top layer. As a result, the three bilayer coatings exhibit soft colors while achieving subambient cooling with temperature drops of up to 1.5 °C. This fluorescence-enhancement strategy may pave the way for preparing highly efficient radiative cooling coatings with tunable colors.

X. Ma, Y. Fu, D. Liu, D. Lei
Department of Materials Science and Engineering
Center for Functional Photonics, and Hong Kong Branch of National
Precious Metals Material Engineering Research Centre
City University of Hong Kong
83 Tat Chee Avenue, Kowloon, Hong Kong 999077, China
E-mail: dangylei@cityu.edu.hk

N. Yang
Department of Civil and Environmental Engineering
The Hong Kong Polytechnic University
Hung Hom, Kowloon, Hong Kong 999077, China
J.-G. Dai
Department of Architecture and Civil Engineering

City University of Hong Kong 83 Tat Chee Avenue, Kowloon, Hong Kong 999077, China

The ORCID identification number(s) for the author(s) of this article can be found under https://doi.org/10.1002/adom.202303296

© 2024 The Authors. Advanced Optical Materials published by Wiley-VCH GmbH. This is an open access article under the terms of the Creative Commons Attribution-NonCommercial-NoDerivs License, which permits use and distribution in any medium, provided the original work is properly cited, the use is non-commercial and no modifications or adaptations are made.

DOI: 10.1002/adom.202303296

1. Introduction

Cooling of confined spaces, such as buildings and vehicles, is of great significance to keep the thermal comfort for human beings, while conventional compressionbased air conditioners are energy-intensive and environmentally harmful, aggravating the global warming and energy crisis. Recently, passive daytime radiative cooling has been investigated worldwide due to its potential for space cooling without energy consumption and greenhouse gas emissions.[1-5] To achieve daytime radiative cooling, both high effective reflectance under direct sunlight (0.3-2.5 µm) and high thermal emissivity in the region of atmospheric transparent window (8-13 µm) are required, through which a terrestrial object (≈300 K) dissipates heat by radiating to the cold outer space (3 K).[6-8]

Versatile materials and structures, including multilayered photonic structures, [9-12] metamaterials, [13-15] porous structures, [7,16,17] and polymer-dielectric composites [16-19] have been proposed for realizing efficient radiative cooling,

among which polymer-dielectric composites exhibit a variety of advantages, such as low-cost fabrication, scalable production, and high cooling efficiency, making them excellent candidates for real-world applications. A polymer-dielectric cooling coating usually consists of a polymer matrix (PMMA, PDMS, TPX, PVA, etc.)^[20–25] with high thermal radiation and dielectric fillers (TiO₂, Al₂O₃, SiO₂, BaSO₄, etc.)^[21,26–28] for high solar reflectance and practical functionalities. However, to maximize the solar reflectance, a white appearance was always deployed based on multiple Mie scattering by the broad size distribution of fillers, which is aesthetically bored.

Colored radiative cooling coatings have been investigated to weaken the light pollution from the super-white coating and address the aesthetical demands through colored pigments, photonic structures, or fluorescent phosphors. [29–35] Unfortunately, most colored pigments absorb visible light significantly and convert it to non-radiative thermal energy, compromising the cooling effect. Notably, visible light counts for almost half of the total solar energy (i.e., $\approx 500~W~m^{-2}$), which can heat deep-colored objects far more than the typical cooling capacity of outgoing infrared radiation ($\approx 120~W~m^{-2}$). Therefore, pigment-based colored cooling coatings are facing a paradox between color saturation and cooling effect. [35] To minimize and even



www.advancedsciencenews.com



www.advopticalmat.de

eliminate the absorption-induced heat gain under coloration, photonic structures have been investigated including optimized multilayer films for narrowing absorption linewidth and periodic micro/nanostructures for light diffraction/interference. However, the equipment-intensive manufacture processes like deposition and lithography are usually required for sophisticated periodic structures, which is costly and incompatible with large-scale fabrication.[34] Regarding this issue, a fluorescentassisted method has been proposed and investigated both theoretically and experimentally to reduce solar absorption and solve the above dilemma of colored radiative cooling.[36-39] Compared to the non-fluorescent pigment, fluorescent materials could reemit the absorbed light to photons at longer wavelengths, weakening the solar heating introduced by coloration. Meanwhile, it is compatible with the polymeric-dielectric composites and is cost-effective, which is promising for large-scale real-world applications. Various factors including the photoluminescence quantum yield (PLQY), Stokes shift, fluorescent spectra, and external quantum yield have been considered for optimizing the fluorescence-based colored cooling coatings, while achieving subambient cooling effect under peak solar irradiation still remains challenging due to the non-ideal photoluminescent (PL) properties.[40-42] Typically, high PLQY and small Stokes shift of fluorescent pigment are favorable in the fluorescence-assisted cooling coating.[42] Perovskite nanocrystals have been employed as high-performance fluorescent fillers for cooling coatings due to their high PLQY.[43,44] However, perovskite nanocrystals are sensitive to water and oxygen, which gives rise to long-term stability concerns. In addition, the toxicity of lead could cause apprehension from an environmental perspective. Rare-earth ions doped phosphors are also promising candidates for colored fluorescent-assisted cooling since they combine high PLQY, large color rendition index, and high resistance to degradation in the water-based polymer matrix.[38] Beyond the intrinsic PL properties, the Purcell effect could be introduced for further improvement when the phosphors are embedded into a polymerdielectric coatings. Under Mie resonances of surrounding dielectric fillers, the local dielectric environment of the fluorescent pigment is modified, and the PL lifetime would be shortened.[20] More luminous photons would be re-emitted within the same time and improve the backward power intensity, that is, the effective solar reflectance (ESR). However, only Purcell enhancement in white cooling coatings was reported at the status quo, in which only UV light was utilized to excite the PL. Besides, part of UV light is in fact competitively absorbed by the nanosized TiO₂ fillers instead of fluorescent pigments in white cooling coatings.[20,42] The Purcell effect is expected to be more efficient in ESR improvement if more light is absorbed by the fluorescent pigments. Therefore, Purcell enhancement would be superior in colored cooling coatings than in white ones since the visible light counts ≈11 times the power intensity more than the UV light within the solar irradiation, while further insights to the modified PL properties in the fluorescence-based colored coatings are

In this work, a series of fluorescent-assisted colored coatings were fabricated and investigated on their optical properties and cooling capacities. Bilayer structures combining a white bottom layer and a top-colored layer were applied to improve both solar reflectance and coloration. Both layers are composed of a polymer

matrix (poly-styrene-acrylic) and two dielectric fillers. The bottom layer contains ${\rm TiO_2}$ nanoparticles and hollow glass spheres for primary solar reflection and thermal emission, while the top layer consists of ${\rm SiO_2}$ microspheres and phosphors (${\rm Sr_2Si_5N_8:Eu^{2+}}$, ${\rm Y_3Al_5O_{12}:Ce^{3+}}$, and (Ba,Sr)SiO₄:Eu²⁺, for red, yellow, and green color, respectively). Based on the scattering analysis and PL characterization, the size effect of ${\rm SiO_2}$ microspheres in the top layer was investigated to effectively boost Purcell enhancement and reduce UV absorption from the bottom white layer. Finally, cooling capacity was evaluated and compared by outdoor field test, in which sub-ambient cooling could be observed. Our bilayer color coatings have revealed the potential of Purcell-enhanced fluorescence on improving solar reflectance under aesthetic requirement and pave the way to entitle colored radiative cooling with sub-ambient cooling capacity.

2. Results and Discussion

To present color, an object needs to reflect specific parts of visible light while absorb/transmit the other parts, resulting in solar heating of the object and the underlying substrate. As shown in Figure 1a, compared to the non-fluorescent pigments that convert the absorbed visible light to non-radiative energy, fluorescent materials can emit the absorbed light to photons with longer wavelengths, making them more desired for colored cooling coating. Moreover, the re-emitted light would help configure the color in vision and further increase the saturation. To achieve a radiative cooling effect, high thermal emissivity is required especially in the range of atmospheric window (8-13 µm) to transfer heat to the space. Two different thermal radiation features: selective and broadband emission were commonly proposed. The selective coating could suppress parasitic heat absorption, while the broadband coating shows larger cooling power even under moderate temperature reduction (Figure S1, Supporting Information). Considering the color-induced solar heating, the temperature reduction of colored cooling coatings would be less or even negative, in which the broadband emission is favored for better cooling performance (Figure 1b).

Upon the above spectral requirement, we adopted a bilayer polymeric composite as the colored cooling coating, as shown in Figure 1c. The employed polymer matrix is poly-styrene-acrylic, providing a framework for the broadband radiator. Commercial white powders, TiO2 nanoparticles, and hollow glass microspheres were applied as the fillers in the bottom layer to provide the white base. High reflectance in the visible and NIR range can be observed (Figure S2, Supporting Information). However, the intrinsic absorption of TiO2 endows poor reflection in the UV range. Incorporating SiO₂ microspheres in the top layer could effectively scatter the UV light, as well as the visible and NIR light, depending on their sizes. To investigate the impact of the SiO₂ microspheres' diameter on the solar reflectance, white bilayer coatings based on SiO₂ microspheres with average diameters $\approx 2, 5$, and 10 µm were first fabricated. Although the coating with 2 µm-sized SiO₂ shows the highest UV reflectance, the total solar reflectance values of the three coatings are 91.8%, 92.6%, and 89.8%, respectively (Figure S3, Supporting Information). Therefore, the SiO₂ spheres with an average diameter of 5 µm was selected as the optimum. Moreover, as shown in Figure S4 (Supporting Information), the bilayer white coatings have a high

conditions) on Wiley Online Library for rules of use; OA articles are governed by the applicable Creative Commons I

www.advancedsciencenews.com

www.advopticalmat.de

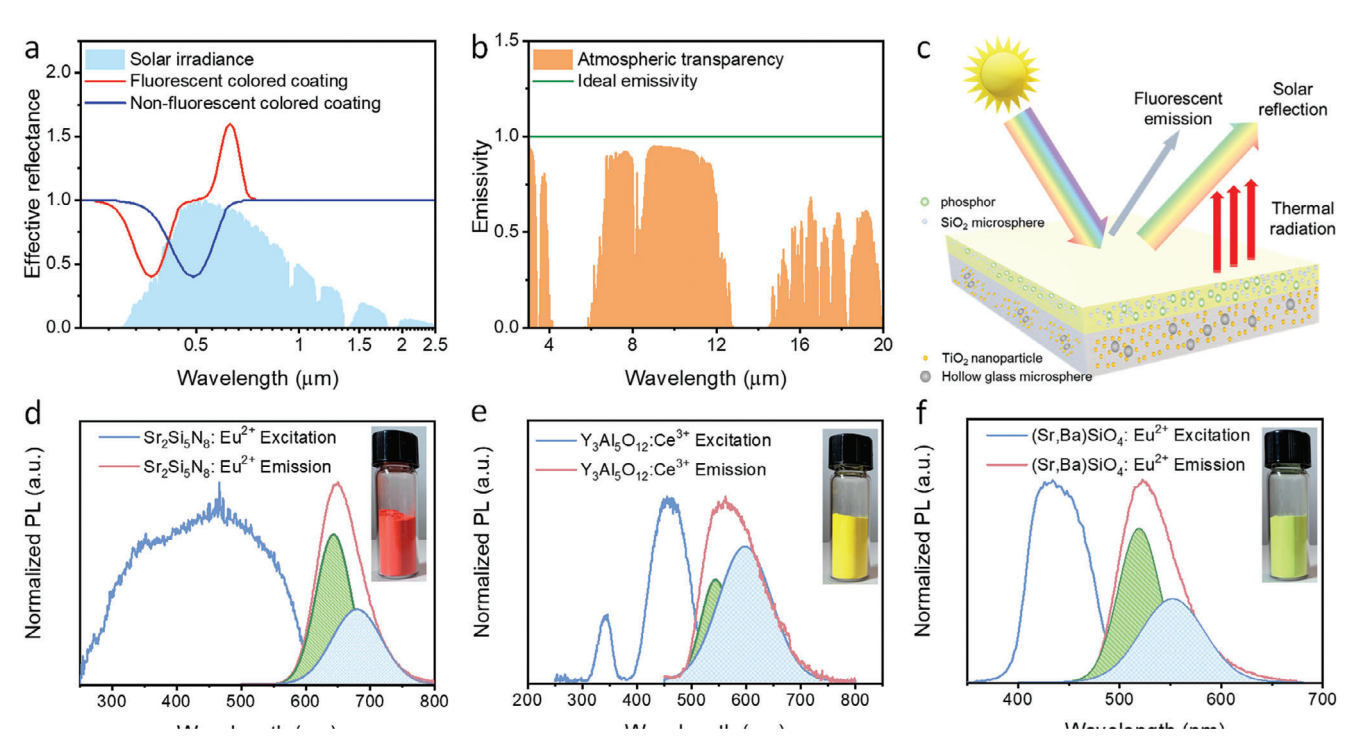


Figure 1. a) Schematic comparison between the effective reflectance spectra for colored radiative cooling coatings with (red line) and without (blue line) fluorescence contribution. The normalized AM1.5 spectral solar irradiance is also plotted for reference. b) Infrared thermal emittance spectrum of an ideal broadband radiative cooler (green line). The atmospheric transmittance spectrum is also plotted as a reference. c) Schematic of our proposed fluorescence-assisted colored bilayer radiative cooling coating. The bottom layer is a white coating containing TiO₂ nanoparticles and hollow glass microspheres in poly-styrene-acrylic, and the top layer consists of fluorescent phosphors and SiO₂ microspheres. d–f) Excitation and emission spectra of a red phosphor (d), a yellow phosphor (e), and a green phosphor (f). Insets are the corresponding optical images of these phosphors in powder.

infrared emissivity of over 90% (90.1%, 90.6%, and 90.9% for 2, 5, and 10 μ m SiO₂), which is slightly higher than that of the TiO₂ bottom layer (89.5%).

rare-earth-doped Three phosphors, red phosphor Sr₂Si₅N₈:Eu²⁺, yellow phosphor Y₃Al₅O₁₂:Ce³⁺, and green phosphor (Ba,Sr)SiO₄:Eu²⁺ were employed as the colored fluorescent material. Their excitation and emission spectra are shown in Figure 1d-f, indicating that they could be excited by both UV and visible light and could emit light with longer wavelengths. It should be noted that the emission spectra of the three phosphors can be fitted into two Lorenz peaks attributing to the atomic arrangement. For Sr₂Si₅N₈:Eu²⁺ and (Ba,Sr)SiO₄:Eu²⁺, as illustrated in Figure S6 (Supporting Information), two kinds of host Sr²⁺ ion sites (Sr²⁺ 1 and Sr²⁺ 2) experiencing different crystal field strengths could be occupied by the Eu²⁺ ions (Eu²⁺ 1 and Eu²⁺ 2), leading to the excited states $4f^{6}5d^{1}$ of Eu²⁺ locate at different energy levels. [45–50] For $Y_3Al_5O_{12}$: Ce^{3+} , though the doped Ce³⁺ experiences the same crystal strength, the PL emission peak shows a two-peak feature since the 4f state of Ce^{3+} is split into two components (${}^{2}F_{5/2}$ and ${}^{2}F_{7/2}$) by spin-orbit interaction.^[51–54] The crystal structure and energy transfer mechanism are shown in Figure \$7 (Supporting Information).

Besides the UV reflectance improvement, SiO₂ microspheres in the top layer can also manipulate the PL emission of phosphors. It has been demonstrated that the PL decay of the phosphors can be reduced after being introduced into the TiO₂-based coating, indicating a Purcell effect in the coating system. However, considering the strong UV absorption and non-spherical

geometry of the TiO₂ nanoparticles, SiO₂ microspheres were selected to provide better Mie resonance and local field modification that endows the Purcell effect. Similar to TiO2 nanoparticles, SiO₂ microspheres can also scatter light with different wavelengths regarding the diameters. Figure 2a shows the calculated scattering spectra of SiO₂ microspheres with diameters of 2, 5, and 10 µm in the polymer matrix. We can observe that large-sized SiO₂ microspheres scatter light at longer wavelengths more efficiently, providing Mie scattering over all the PL emission ranges of three phosphors. Electric field enhancement at the emission peaks of phosphors surrounding SiO₂ microspheres with different sizes is revealed in Figure 2b under the excitation of a horizontal emission dipole. The presence of SiO₂ microspheres performs observable field modification of the dipole, indicating the modulation capacity for the PL process of the phosphors. Further, the PL lifetimes of each phosphor in coatings with SiO₂ microspheres of different average diameters were characterized. As illustrated in Figure 2d,e, all phosphors in the coating exhibit an obvious decrease in PL lifetime. As mentioned above, the PL emission spectra of Sr₂Si₅N₈:Eu²⁺ and (Ba,Sr)SiO₄:Eu²⁺ can be fitted by two peaks originating from two kinds of Eu²⁺ ions experiencing different crystal fields. Nevertheless, since the monitoring wavelength locates at the overlapping region of two emission peaks, we adopted single exponential form for lifetime fitting. As for Y₃Al₅O₁₂:Ce³⁺, only one decay channel can be extracted from the low-energy excitation state (i.e., ²D_{3/2} in Figure S7, Supporting Information), which also requires single exponential lifetime fitting. The fitted results for all phosphors with and without SiO2

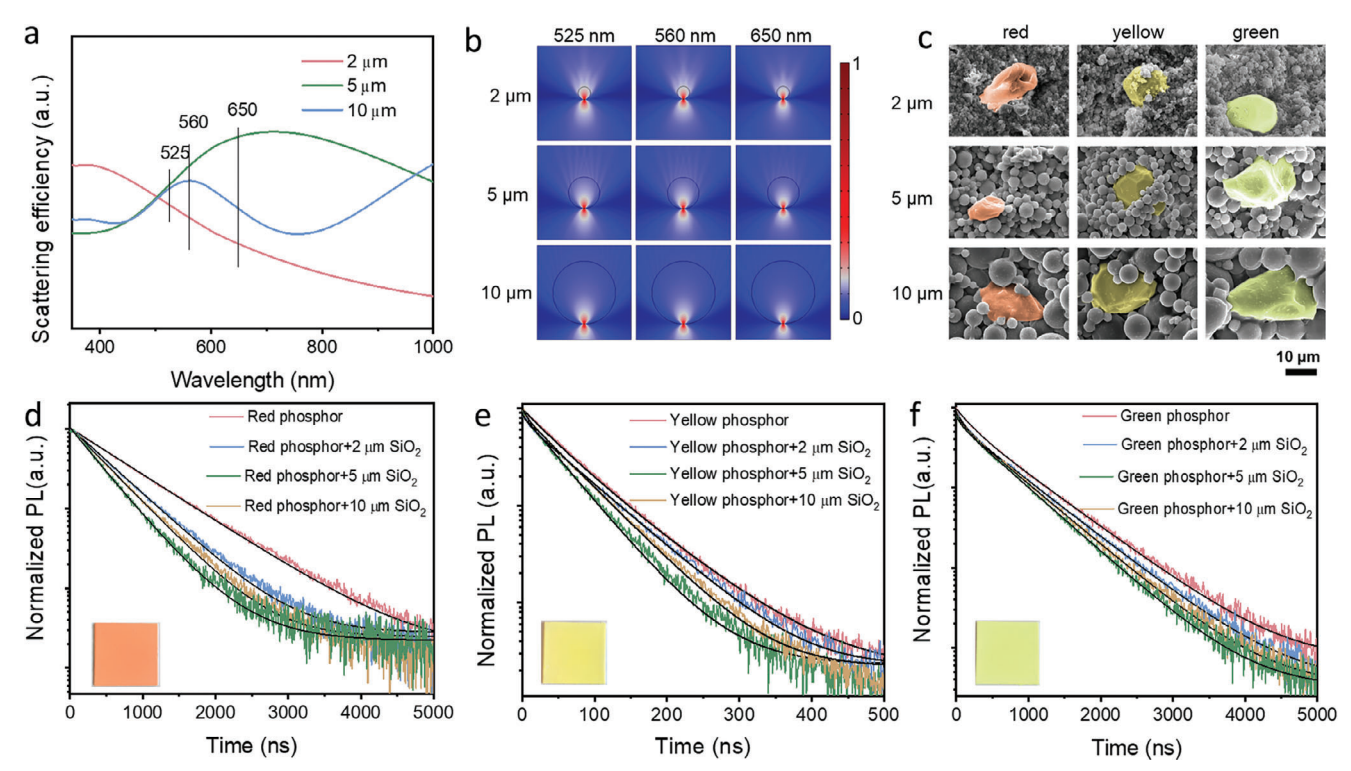


Figure 2. a) Simulated scattering efficiencies of SiO_2 microspheres with varied diameters in the polymer matrix. b) Electric field distribution profiles in the same SiO_2 microspheres at $\lambda=525$, 560, and 650 nm as marked in (a). The excitation source is a horizontal electric dipole adjacent to the bottom side of the SiO_2 microspheres. The surrounding dielectric is set to be our polymer matrix (poly-styrene-acrylic) with a scattering boundary condition. c) Cross-sectional SEM images of colored coatings with SiO_2 microspheres of different diameters and phosphors of different colors. The false-colored regions correspond to the three phosphors. Detailed size distributions of SiO_2 microspheres are shown in Figure S8 (Supporting Information). d–f) PL lifetime spectra of pure phosphors and that in three cooling coatings with SiO_2 microspheres at different diameters. Each solid line represents a single exponential fitting of the experimental data.

microspheres are shown in Tables S1–S3 (Supporting Information). It can be observed that the 5 μm SiO₂ microspheres reveal stronger lifetime reduction than other sizes.

As the PL lifetime is reduced by surrounding SiO_2 microspheres, the electrons would be released from the excited energy level faster, leading to higher competition to non-radiative decay. Therefore, the PLQY is improved through the Purcell effect. In addition, more incident photons will be absorbed to excite electrons since the electron population of excited energy level reduces. To further evaluate the influence of Purcell effect on the PL of phosphors when integrated into the coating, we have defined the absorption of excitation light (*Abs*), PLQY, and power yield (*PY*) as follows:

Abs =
$$\int_{\lambda_{\text{ex, min}}}^{\lambda_{\text{ex, min}}} hc \frac{I_{\text{ref}}(\lambda) - I_{\text{PL}}(\lambda)}{\lambda I_{\text{ref}}(\lambda)}$$
(1)

$$PLQY = \frac{\int_{\lambda_{\text{em, max}}}^{\lambda_{\text{em, max}}} I_{\text{PL}}(\lambda) - I_{\text{ref}}(\lambda)}{\int_{\lambda_{\text{em, min}}}^{\lambda_{\text{ex, max}}} I_{\text{ref}}(\lambda) - I_{\text{PL}}(\lambda)}$$
(2)

$$PY = \frac{\int_{\lambda_{\text{em,min}}}^{\lambda_{\text{em,min}}} hc^{\frac{I_{\text{PL}}(\lambda) - I_{\text{ref}}(\lambda)}{\lambda}}}{\int_{\lambda_{\text{ex,min}}}^{\lambda_{\text{ex,max}}} hc^{\frac{I_{\text{ref}}(\lambda) - I_{\text{PL}}(\lambda)}{\lambda}}}$$
(3)

where $\lambda_{\rm ex,min}\sim\lambda_{\rm ex,max}$ and $\lambda_{\rm em,min}\sim\lambda_{\rm em,max}$ are the wavelength range of excitation and emission of phosphors, respectively. $I_{\rm PI}(\lambda)$ and $I_{\rm ref}(\lambda)$ are the measured photon intensity with and without samples, respectively. h and c are Planck's constant and the speed of light, respectively. To identify the impact of surrounding SiO₂ microspheres on the PL behaviors in the coating, a control group with a top layer comprised of only phosphors in polymer is also prepared and compared. Note that an average diameter of 5 µm is selected due to the superior Purcell effect as indicated in Figure 2 and Tables S1-S3 (Supporting Information). As shown in Figure 3a-c, the absorptions of excitation light are increased by 13-25%, 8-26%, and 7-22% for red, yellow, and green phosphors, respectively. The absorption enhancement can be attributed to the multiple scattering of the spherical Mie resonators that can bring the light back to the phosphors. Similar enhancement on Abs can be attributed to the comparable electric field modulation of 5 µm SiO₂ microspheres at three peak wavelengths of three phosphors (Figure 2b). Moreover, PLQYs of the phosphors at the presence of SiO₂ microspheres are also enhanced due to the Purcell effect, as shown in Figure 3d-f. PLQYs of all three phosphors are generally higher than the original value (81%, 95.8%, and 91.0% for red, yellow, and green phosphors). For yellow and green phosphors, the PLQYs are increased ≈0.2-0.8%, while the average enhancement of the red phosphor reaches over 10%. The reason is straightforward that

21951071, 0, Downloaded from https://onlinelibrary.wiley.com/doi/10.1002/adom.202303296 by City University Of Hong Kong, Wiley Online Library on [26.05/2024]. See the Terms

ditions) on Wiley Online Library for rules of use; OA articles are governed by the applicable Creative Commons

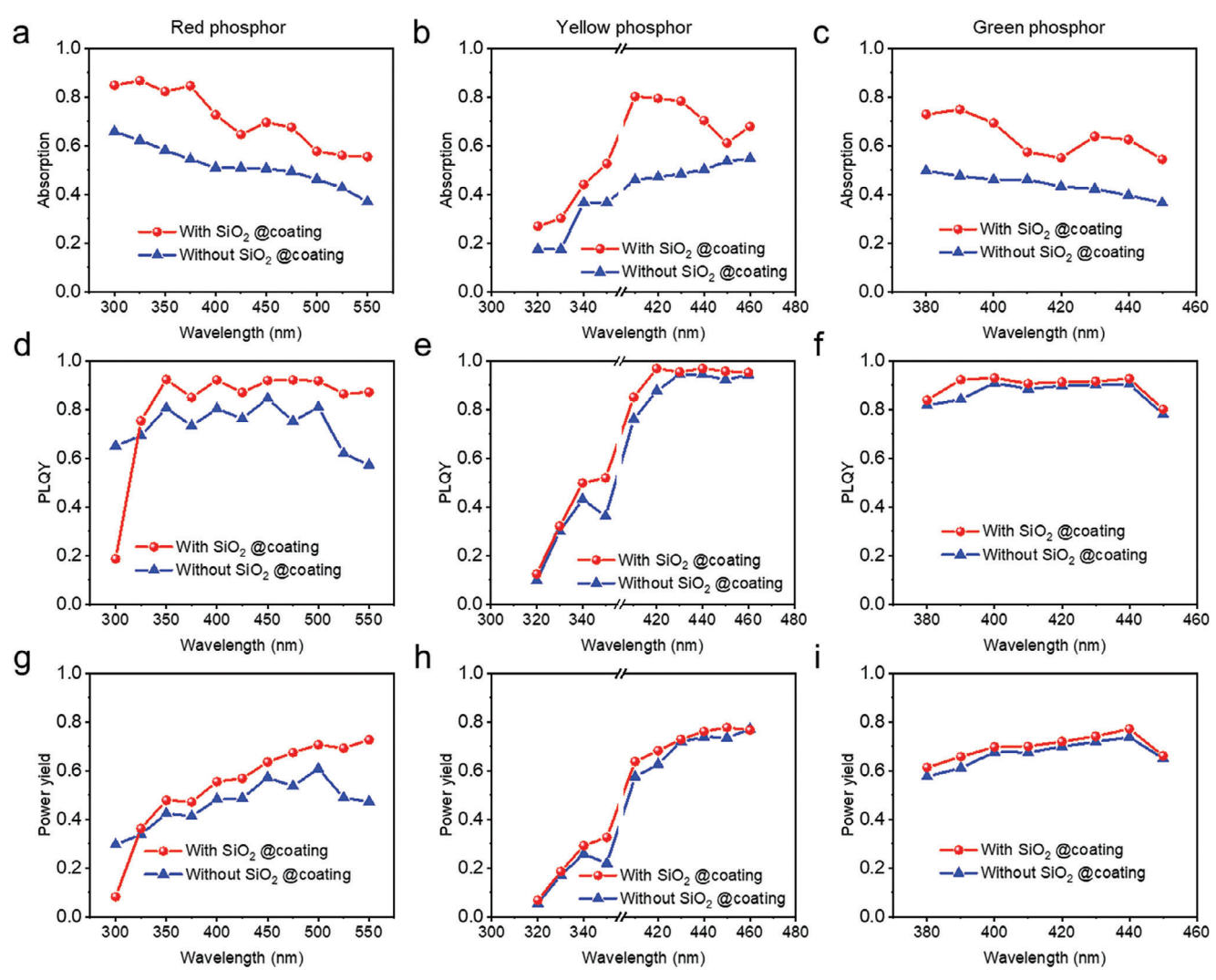


Figure 3. a–c) Absorption spectra of the red (a), yellow (b) and green (c) phosphors in the coatings with (red dots) and without SiO₂ microspheres (blue dots). d,e) Corresponding PLQYs and g–i) PY of the three phosphors.

the pristine lower PLQY of red phosphors indicates considerable non-radiative decay, which can be efficiently suppressed by Purcell effect. No obvious derivations are found for yellow and green phosphors since the high pristine PLQYs limit the Purcell effect. However, the absorption within the excitation range is obviously improved for all three phosphors. It means that more sunlight within the excitation range can be converted to photons at longer wavelengths with improved PLQY, revealing the huge potential for color manipulation under minimized light-heat conversion. The PY represents the energy efficiency of radiative photon conversion and reveals a similar trend of PLQY since the Stokes shift is fixed at the measuring wavelength, the upper limit of PY can be obtained at PLQY = 100% and higher PLQY can help PY reach the upper limit. Thus, the surrounding SiO₂ microparticles can efficiently improve the absorption, PLQY, and PY of phosphors, thereby enhancing coloration and the PL contribution in colored radiative cooling coatings.

Normally, radiative cooling coatings without fluorescent materials can gradually approach the largest solar reflectance with

the increasing of their thickness, ascribing to the improved multiple scattering. However, increasing the thickness of the colored top layer in our fluorescence-assisted coatings would slightly increase the absorption within the excitation wavelength (i.e., reduced overall solar reflectance), which can be ascribed to the nonperfect energy conversion from the absorbed short-wavelength solar light to the long-wavelength photoluminescence emission. The non-perfect conversion efficiency was caused by the nonunity PLQY and intrinsic Stokes shift of fluorescent materials. The paradox between color saturation and radiative cooling becomes apparent again with a thick top layer. Once the solar reflectance approaches its maximum, the multiple scattering cannot improve the solar reflectance while the absorption induced by phosphors will reduce the ESR when further increasing toplayer thickness. Therefore, the overall solar reflection is supposed to be first improved and then reduced along increasing the toplayer thickness. The turning point is located at the thickness when the solar reflectance approaches its maximum for coatings without phosphors. As illustrated in Figure S9 and Table S4



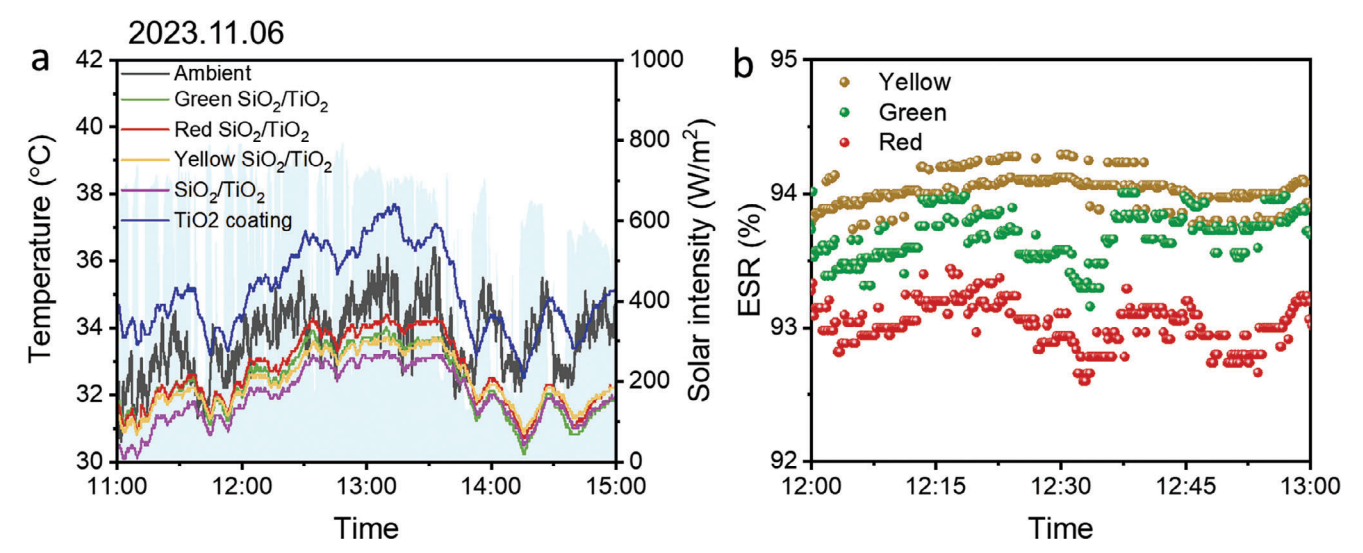


Figure 4. a) Recorded temperature curves of ambient air (gray), a single-layer TiO₂ coating (blue), a SiO₂/TiO₂ bilayer white coating (purple), and three bilayer colored coatings (red, yellow, and green). The diameters of SiO₂ microspheres in the top layers of all bilayer coatings 5 μm. b) Calculated ESR of the bilayer colored coatings corresponding to SiO_2 microspheres with diameters of 5 μ m.

(Supporting Information), the reflectance of bilayer coatings in UV and NIR regions significantly increases as the thickness of the top SiO₂ layer increases, reaching a saturation point at a thickness of 150 µm.

The cooling capacity of our bilayer-colored cooling coatings was evaluated by an outdoor field test in Hong Kong. The setup and weather condition are shown in Figures S10-S12 (Supporting Information). Notably, the ambient temperature is measured through a thermocouple placed in a louvered box mimicking the Stevenson screen to avoid direct sunlight heating and enable thermal convection with ambient air through passive ventilation (Figure S13, Supporting Information). The colored and white top layers were fabricated on the TiO₂ bottom white coating on concrete boards. All samples were placed on top of the thermally insulated boxes during the field test. The measured temperatures of all samples are shown in Figure 4a. As the solar intensity increases at noontime, white bilayer coatings can reduce the temperature up to 2°C compared with the ambient air, and three colored coatings reduce the temperature of 1.5, 1.2, and 0.8°C, respectively (Figure S14, Supporting Information). While the temperature of the bottom TiO₂-based white coating is ≈1.8°C higher than the ambient. Yellow coatings perform lower temperature at sun irradiation due to the smallest Stokes shift of 95 nm (Figure 1e) and highest PLQY (Figure 3e). The ESR of all coatings is fitted by the solar reflectance-temperature relations among all non-fluorescent coatings as [36,42]

$$T = a \cdot ESR + b \tag{4}$$

where a and b are environmental parameters fitted from the solar reflectance as well as the temperature of white base (TiO₂ bottom) and white bilayer coatings. The fitted results of the colored coatings, as shown in Figure 4b, are 93%, 94%, and 93.6% for red, vellow, and green phosphors, indicating potential cooling power of 38.1, 45.6, and 42.6 W m⁻², respectively. The red coatings show lower ESR since large Stokes shift and low PLQY induce lower PY. Compared to those non-fluorescent-colored coatings, our Purcell-enhanced fluorescent strategy can introduce color without significant sacrifice on solar reflectance.

3. Conclusion

In this work, we designed and fabricated fluorescence-assisted colored bilayer cooling coatings using rare-earth doped phosphors. The influence of phosphors' optical properties on the cooling effect of the colored coatings was investigated. By introducing SiO₂ microspheres with appropriate size distributions in the top layer, the ESR of the bilayer white coating could be maximized to 94.8%, higher than the TiO₂-based white bottom layer. SiO₂ microspheres can also modify the surrounding electromagnetic environment of phosphors and accelerate their spontaneous emission process through the Purcell enhancement mechanism. Significant improvements in PLQY and energy conversion efficiency were observed. Moreover, the improved absorption within the excitation range enables potential color manipulation without incurring heat gain. Field tests further demonstrated that higher Purcell enhancement and SiO2 with proper diameters are preferred to improve the cooling performance, indicating a feasible solution to maintain solar reflection with coloration. Our work has provided a detailed comprehension of the optical properties of phosphors and paved the way for the wider application of fluorescent-assisted colored cooling coatings.

4. Experimental Section

Materials: Hollow glass microspheres were purchased from 3M. $Sr_2Si_5N_8$: Eu^{2+} , $Y_3Al_5O_{12}$: Ce^{3+} , and $(Ba,Sr)SiO_4$: Eu^{2+} were bought from Shenzhen Looking Long Technology. Poly-styrene-acrylic matrix was bought from BASF Co. Ltd. Polycarboxylate sodium salt was employed as the dispersant agent. The Polyurethane associative served as the suspending agent. The anti-foaming agent was mineral oil. The film forming agent www.advancedsciencenews.com

ADVANCED OPTICAL MATERIALS

www.advopticalmat.de

was 9Z-Dodecenyl acetate. The leveling agent was Polyurethane. All agents were purchased from Guang Zhou Run Hong Chemical.

Sample Preparation: The preparation of TiO_2 was proceeded as follows: 20 g poly-styrene-acrylic emulsion, 12 g TiO_2 nanoparticles, and an appropriate amount of water were first mixed in a 50 mL beaker with continuous stirring, followed by the additions of dispersant agent, suspending agent, and leveling agent. The mixture was stirred at 800 rpm for an hour. Then the stirring speed was turned down to 400 rpm and 3 g hollow glass microspheres, 0.4 g anti-foaming agent, and 1 g film-forming agent were added. After 30 min of stirring, the mixture was sprayed evenly on the cement board with a spray gun under a pressure of 5 MPa.

The preparation of the ${\rm SiO_2}$ top layer with phosphor was proceeded as follows: 20 g poly-styrene-acrylic emulsion, 25 g ${\rm SiO_2}$ microparticles, 3.9 g phosphor, and an appropriate amount of water were first mixed in a 50 mL beaker with continuous stirring, followed by the additions of dispersant agent, suspending agent and leveling agent. The mixture was stirred at 800 rpm for an hour. Then the stirring speed was turned down to 400 rpm and 0.4 g anti-foaming agent and 1 g film-forming agent were added. After 30 min of stirring, the mixture was sprayed evenly on the cement board with a spray gun under a pressure of 5 MPa.

Sample Characterization and Field Test: The reflectance spectra of the coating were measured on a PerkinElmer Lambda 1050+ UV/VIS/NIR Wide Band Spectrometer equipped with an integrating sphere. Excitation spectra, emission spectra, PL lifetime, and PLQY of pure phosphors/fluorescent cooling coatings were collected on an Edinburgh Instruments FLS900 Fluorescence spectrometer. The cross-section of the coating was characterized by an FEI Quanta 450 Field-Emission Scanning Electron Microscopy under a voltage of 15 kV. The XRD patterns were measured on D2 PHASER XE-T X-ray Diffractometer System. The infrared emissivity of cooling coatings was measured on a Fourier transform infrared spectrometer (FT-IR Spectrometer, Spectrum 100, PerkinElmer) coupled with a diffusive gold-coated integrating sphere. The scanning range was from 650 to 4000 cm⁻¹ with a spectral resolution of 4 cm⁻¹, and a total of 16 scans were collected. The real-time temperatures of coatings were recorded on a MEMORY HILOGGER LR8431-30 multichannel temperature collector with K-type thermocouples. The solar intensity and relative humidity were recorded by an accurate pyranometer (EKO MS-802) and a mini weather station. The cooling power of three colored coatings is estimated with the ESR and infrared emissivity under a peak solar irradiation of \approx 750 W m⁻² and an infrared cooling potential of \approx 100 W m⁻².

Supporting Information

Supporting Information is available from the Wiley Online Library or from the author.

Acknowledgements

The authors acknowledge the financial support by the City University of Hong Kong through the ARG project (9667246), the Research Grants Council of Hong Kong through a GRF project (15223120) and a CRF project (C5051-22GF), the Innovation and Technology Commission of Hong Kong through an ITF grant (MHP/162/22), the Centre for Functional Photonics of the City University of Hong Kong, and the Hong Kong Branch of National Precious Metals Material Engineering Research Center (ITC Fund).

Conflict of Interest

The authors declare no conflict of interest.

Author Contributions

X.M. performed conceptualization, investigation, and writing. Y.F. performed investigation and writing. D.L. and N.Y. performed the investigation. D.L. and J.-G.D. performed supervision and revision. X.M. thanks Xin

Zhao for XRD measurements and Arsenii Portniagin for preliminary PL lifetime measurements. D.L. thanks Andrey L. Rogach for providing the use of a PL lifetime spectrometer and Ying Liu for a brief proofreading.

Data Availability Statement

The data that support the findings of this study are available from the corresponding author upon reasonable request.

Keywords

bilayer coating, colored coating, fluorescent material, purcell enhancement, radiative cooling

Received: January 26, 2024 Revised: April 24, 2024 Published online:

- [1] Z. Li, Q. Chen, Y. Song, B. Zhu, J. Zhu, Adv. Mater. Technol. 2020, 5, 1901007
- [2] X. Lu, P. Xu, H. Wang, T. Yang, J. Hou, Renew. Sust. Energy Rev. 2016, 65, 1079.
- [3] J. Mandal, Y. Yang, N. Yu, A. P. Raman, Joule 2020, 4, 1350.
- [4] M. Santamouris, J. Feng, Buildings 2018, 8, 168.
- [5] D. Zhao, A. Aili, Y. Zhai, S. Xu, G. Tan, X. Yin, R. Yang, Appl. Phys. Rev. 2019. 6. 021306.
- [6] X. Li, J. Peoples, Z. Huang, Z. Zhao, J. Qiu, X. Ruan, Cell Rep. Phys. Sci. 2020, 1, 100221.
- [7] J. Mandal, Y. Fu, A. C. Overvig, M. Jia, K. Sun, N. N. Shi, H. Zhou, X. Xiao, N. Yu, Y. Yang, *Science* 2018, 362, 315.
- [8] A. P. Raman, M. A. Anoma, L. Zhu, E. Rephaeli, S. Fan, *Nature* 2014, 515, 540.
- [9] N. N. Shi, C.-C. Tsai, M. J. Carter, J. Mandal, A. C. Overvig, M. Y. Sfeir,
 M. Lu, C. L. Craig, G. D. Bernard, Y. Yang, Light: Sci. Appl. 2018, 7, 37.
- [10] M. Lee, G. Kim, Y. Jung, K. R. Pyun, J. Lee, B.-W. Kim, S. H. Ko, Light: Sci. Appl. 2023, 12, 134.
- [11] H. Ma, K. Yao, S. Dou, M. Xiao, M. Dai, L. Wang, H. Zhao, J. Zhao, Y. Li, Y. Zhan, Solar Energy Mater. Solar Cells 2020, 212, 110584.
- [12] D. Chae, M. Kim, P.-H. Jung, S. Son, J. Seo, Y. Liu, B. J. Lee, H. Lee, ACS Appl. Mater. Interfaces 2020, 12, 8073.
- [13] Y. Zhai, Y. Ma, S. N. David, D. Zhao, R. Lou, G. Tan, R. Yang, X. Yin, Science 2017, 355, 1062.
- [14] C. Zou, G. Ren, M. M. Hossain, S. Nirantar, W. Withayachumnankul, T. Ahmed, M. Bhaskaran, S. Sriram, M. Gu, C. Fumeaux, Adv. Opt. Mater. 2017, 5, 1700460.
- [15] S. Jeong, C. Y. Tso, Y. M. Wong, C. Y. Chao, B. Huang, Solar Energy Mater. Solar Cells 2020, 206, 110296.
- [16] D. Li, X. Liu, W. Li, Z. Lin, B. Zhu, Z. Li, J. Li, B. Li, S. Fan, J. Xie, Nat. Nanotechnol. 2021, 16, 153.
- [17] A. Leroy, B. Bhatia, C. C. Kelsall, A. Castillejo-Cuberos, H. M. D. Capua, L. Zhao, L. Zhang, A. Guzman, E. Wang, Sci. Adv. 2019, 5, eaat9480.
- [18] Y. Liu, A. Bai, Z. Fang, Y. Ni, C. Lu, Z. Xu, Materials 2019, 12, 1208.
- [19] Y. Chen, B. Dang, J. Fu, C. Wang, C. Li, Q. Sun, H. Li, Nano Lett. 2020, 21, 397.
- [20] X. Xue, M. Qiu, Y. Li, Q. Zhang, S. Li, Z. Yang, C. Feng, W. Zhang, J. G. Dai, D. Lei, Adv. Mater. 2020, 32, 1906751.
- [21] X. Li, J. Peoples, P. Yao, X. Ruan, ACS Appl. Mater. Interfaces 2021, 13, 21733
- [22] H. Zhang, K. C. Ly, X. Liu, Z. Chen, M. Yan, Z. Wu, X. Wang, Y. Zheng, H. Zhou, T. Fan, Proc. Natl. Acad. Sci. U. S. A. 2020, 117, 14657.

www.advancedsciencenews.com www.advopticalmat.de

- [23] P. Yao, Z. Chen, T. Liu, X. Liao, Z. Yang, J. Li, Y. Jiang, N. Xu, W. Li, B. Zhu, Adv. Mater. 2022, 34, 2208236.
- [24] Z. Yang, H. Sun, Y. Xi, Y. Qi, Z. Mao, P. Wang, J. Zhang, Solar Energy Mater. Solar Cells 2021, 227, 111101.
- [25] K. Zhou, W. Li, B. B. Patel, R. Tao, Y. Chang, S. Fan, Y. Diao, L. Cai, Nano Lett. 2021, 21, 1493.
- [26] Y. Liu, S. Son, D. Chae, P.-H. Jung, H. Lee, Solar Energy Mater. Solar Cells 2020, 213, 110561.
- [27] B. Xiang, R. Zhang, Y. Luo, S. Zhang, L. Xu, H. Min, S. Tang, X. Meng, Nano Energy 2021, 81, 105600.
- [28] S. Y. Jeong, C. Y. Tso, J. Ha, Y. M. Wong, C. Y. Chao, B. Huang, H. Qiu, Renew. Energy 2020, 146, 44.
- [29] Y. Zhu, H. Luo, C. Yang, B. Qin, P. Ghosh, S. Kaur, W. Shen, M. Qiu, P. Belov, Q. Li, *Light: Sci. Appl.* 2022, 11, 122.
- [30] W. Xi, Y. Liu, W. Zhao, R. Hu, X. Luo, Int. J. Therm. Sci. 2021, 170, 107172.
- [31] H. Zhai, D. Fan, Q. Li, Solar Energy Mater. Solar Cells 2022, 245, 111853.
- [32] R. A. Yalçın, E. Blandre, K. Joulain, J. Drévillon, ACS Photon. 2020, 7, 1312.
- [33] Y. Zhang, W.-J. Feng, W. Zhu, X. Shan, W.-K. Lin, L. J. Guo, T. Li, ACS Appl. Mater. Interfaces 2023, 15, 21008.
- [34] W. Li, Y. Shi, Z. Chen, S. Fan, Nat. Commun. 2018, 9, 4240.
- [35] Y. Chen, J. Mandal, W. Li, A. Smith-Washington, C.-C. Tsai, W. Huang, S. Shrestha, N. Yu, R. P. Han, A. Cao, Sci. Adv. 2020, 6, eaaz5413.
- [36] R. Levinson, S. Chen, C. Ferrari, P. Berdahl, J. Slack, Energy Buildings 2017, 152, 752.
- [37] D. Chae, S. Y. Lee, H. Lim, S. Son, J. Ha, J. Park, J. H. Park, S. J. Oh, H. Lee, ACS Appl. Mater. Interfaces 2023, 15, 58274.

- [38] J. Xu, R. Wan, W. Xu, Z. Ma, X. Cheng, R. Yang, X. Yin, Mater. Today Nano 2022, 19, 100239.
- [39] B. Xie, Y. Liu, W. Xi, R. Hu, Mater. Today Energy 2023, 34, 101302.
- [40] R. A. Yalçın, E. Blandre, K. Joulain, J. Drévillon, J. Photon. Energy 2021, 11, 032104.
- [41] S. Min, S. Jeon, K. Yun, J. Shin, ACS Photonics 2022, 9, 1196.
- [42] X. Ma, Y. Fu, A. Portniagin, N. Yang, D. Liu, A. L. Rogach, J.-G. Dai, D. Lei, J. Mater. Chem. A 2022, 10, 19635.
- [43] S. Jeon, S. Son, S. Y. Lee, D. Chae, J. H. Bae, H. Lee, S. J. Oh, ACS Appl. Mater. Interfaces 2020, 12, 54763.
- [44] S. Son, S. Jeon, D. Chae, S. Y. Lee, Y. Liu, H. Lim, S. J. Oh, H. Lee, Nano Energy 2021, 79, 105461.
- [45] I. Baginskiy, R. Liu, C. Wang, R. Lin, Y. Yao, J. Electrochem. Soc. 2011, 158. P118.
- [46] R. Cao, X. Wang, X. Ouyang, Y. Jiao, Y. Li, H. Wan, W. Li, Z. Luo, J. Luminesc. 2020, 224, 117292.
- [47] K. A. Denault, J. Brgoch, M. W. Gaultois, A. Mikhailovsky, R. Petry, H. Winkler, S. P. DenBaars, R. Seshadri, Chem. Mater. 2014, 26, 2275
- [48] X. Piao, K.-i Machida, T. Horikawa, B. Yun, J. Luminesc. 2010, 130, 8.
- [49] K.-S. Sohn, S. Lee, R.-J. Xie, N. Hirosaki, Appl. Phys. Lett. 2009, 95, 121903.
- [50] W. Wu, Z. Zhang, R. Dong, G. Xie, J. Zhou, K. Wu, H. Zhang, Q. Cai, B. Lei, J. Rare Earths 2020, 38, 539.
- [51] Y. Pan, M. Wu, Q. Su, Mater. Sci. Eng. B 2004, 106, 251.
- [52] V. Bachmann, C. Ronda, A. Meijerink, Chem. Mater. 2009, 21, 2077.
- [53] E. Zych, C. Brecher, J. Glodo, J. Phys.: Condens. Matter 2000, 12, 1947.
- [54] H. Yang, Y.-S. Kim, J. Luminesc. 2008, 128, 1570.